Frequency-Hopping Multi-Resolution GPR Microwave Imaging Based on Stochastic Optimization

M. Salucci, L. Poli, N. Anselmi, and A. Massa

Abstract

This work presents an innovative microwave imaging technique for processing wide-band ground penetrating radar (*GPR*) data and solving the subsurface inverse scattering problem. The proposed technique is based on the integration of a customized stochastic solver based on the Particle Swarm Optimizer (*PSO*) with the iterative multi-scaling approach (*IMSA*). Moreover, the *IMSA-PSO* is nested within a frequency-hopping (*FH*) approach in order to exploit the frequency-diversity of *GPR* measurements as an additional source of information for regularizing the subsurface inverse scattering problem. Some preliminary numerical results are shown in order to assess the effectiveness of the proposed methodology, as well as to compare it to a single-resolution (*BARE*) implementation within the same framework.

1 Definitions

1.1 Glossary

- SF: Single-Frequency;
- FH: Frequency-Hopping;
- MF: Multi-Frequency;
- P: Swarm dimension;
- U: Total number of unknowns;
- S: Maximum number of $IMSA$ zooming steps;
- s^{best}: Last performed $IMSA$ zooming step ($s^{best} \leq S$);
- η_{th}: $IMSA$ zooming threshold;
- D_{inv}: Investigation domain;
- D_{obs}: Observation domain;
- L: Side of the investigation domain;
- N: Number of discretization cells in D_{ind};
- V: Number of views;
- M: Number of measurement points;
- F: Number of frequencies considered for the inversion;
- $\mathbf{r}^{(v)} = \left(x^{(v)}, y^{(v)}\right)$: Coordinates of the v-th source ($v = 1, \ldots, V$).
- $\mathbf{r}_m^{(v)} = \left(x_m^{(v)}, y_m^{(v)}\right)$: Coordinates of the m-th measurement point for the v-th view v, ($m = 1, \ldots, M$);
- $\varepsilon_{ra} = \frac{\varepsilon_a}{\varepsilon_0}$: Relative electric permittivity for the upper half-space ($y > 0$);
- σ_a: Conductivity for the upper half-space ($y > 0$);
- $\varepsilon_{rb} = \frac{\varepsilon_b}{\varepsilon_0}$: Background relative electric permittivity;
- σ_b: Background conductivity;
- $E_{inc}^{(v)}(\mathbf{r}_n; f)$: Measured internal incident field inside the n-th cell, for the v-th view at frequency f;
- $\widetilde{E}_{inc}^{(v)}(\mathbf{r}_n; f)$: Computed internal incident field inside the n-th cell, for the v-th view at frequency f;
- $E_{scatt}^{(v)}\left(\mathbf{r}_m^{(v)}; f\right)$: Measured external scattered by the m-th measurement point, for the v-th view at frequency f;
- $\widetilde{E}_{scatt}^{(v)}\left(\mathbf{r}_m^{(v)}; f\right)$: Measured external scattered by the m-th measurement point, for the v-th view at frequency f.

FEDIA Research Center

1.2 Contrast function

The contrast function at frequency f is defined as

$$\tau(\mathbf{r}; f) = \frac{\varepsilon_{eq}(\mathbf{r}) - \varepsilon_{eqb}}{\varepsilon_0} = [\varepsilon_r(\mathbf{r}) - \varepsilon_{rb}] + j\left[\frac{\sigma_b - \sigma(\mathbf{r})}{2\pi f \varepsilon_0}\right]$$

where

- $\mathbf{r} = (x, y)$: position vector;
- $\Re\{\tau(\mathbf{r}; f)\} = [\varepsilon_r(\mathbf{r}) - \varepsilon_{rb}]$;
- $\Im\{\tau(\mathbf{r}; f)\} = \left[\frac{\sigma_b - \sigma(\mathbf{r})}{2\pi f \varepsilon_0}\right]$;
- $\varepsilon_{eq}(\mathbf{r}) = \varepsilon_0 \varepsilon_r(\mathbf{r}) - j\frac{\sigma(\mathbf{r})}{2\pi f}$;
- $\varepsilon_{eqb} = \varepsilon_0 \varepsilon_{rb} - j\frac{\sigma_b}{2\pi f}$;
- $\varepsilon_r(\mathbf{r})$: relative electric permittivity at position $\mathbf{r}$;
- $\sigma(\mathbf{r})$: conductivity at position $\mathbf{r}$;

NOTE: we assume that $\varepsilon_r(\mathbf{r})$ and $\sigma(\mathbf{r})$ are **not frequency dependent** (non-dispersive mediums).

ELEDIA Research Center

1.3 Cost function & unknowns

1.3.1 Single-Frequency (SF) and Frequency-Hopping (FH) approaches

These approaches consider data coming from a single frequency at a time. The functional minimized by the inversion algorithm is defined as

$$\Phi(\mathbf{x}) = \Phi_{state}(\mathbf{x}) + \Phi_{data}(\mathbf{x}) \tag{1}$$

where $\Phi_{state}(\mathbf{x})$ and $\Phi_{data}(\mathbf{x})$ are respectively the data and state terms of the cost function, defined at frequency f as

$$\Phi_{state}(\mathbf{x}) = \frac{\sum_{v=1}^{V}\sum_{n=1}^{N}\left|E_{inc}^{(v)}(\mathbf{r}_n;f) - \widetilde{E}_{inc}^{(v)}(\mathbf{r}_n;f)\right|^2}{\sum_{v=1}^{V}\sum_{n=1}^{N}\left|E_{inc}^{(v)}(\mathbf{r}_n;f)\right|^2} \tag{2}$$

$$\Phi_{data}(\mathbf{x}) = \frac{\sum_{v=1}^{V}\sum_{m=1}^{M}\left|E_{scatt}^{(v)}\left(\mathbf{r}_m^{(v)};f\right) - \widetilde{E}_{scatt}^{(v)}\left(\mathbf{r}_m^{(v)};f\right)\right|^2}{\sum_{v=1}^{V}\sum_{m=1}^{M}\left|E_{scatt}^{(v)}\left(\mathbf{r}_m^{(v)};f\right)\right|^2} \tag{3}$$

The unknowns of the inversion problem are

$$\mathbf{x} = \left\{\tau(\mathbf{r}_n;f); E_{tot}^{(v)}(\mathbf{r}_n;f)\right\} \qquad n=1,...,N; v=1,...,V. \tag{4}$$

The total number of unknowns for FH-based approaches is then given by

$$U_{FH} = 2N(1+V). \tag{5}$$

ELEDIA Research Center

1.4 SNR on time-domain external total field

Since data is collected through a GPR system in time-domain, a white Gaussian noise is applied to the measured total field in time domain. The measured total field in time-domain is corrupted by the desired quantity of noise following this definition of SNR [3]:

$$SNR = 10log_{10}\frac{\sum_{v=1}^{V}\sum_{m=1}^{M}\int_{-\infty}^{\infty}\left|\Psi_{tot}^{(v)}\left(\mathbf{r}_m^{(v)};t\right)\right|^2 dt}{\sum_{v=1}^{V}\sum_{m=1}^{M}\int_{-\infty}^{\infty}\left|\nu^{(v)}\left(\mathbf{r}_m^{(v)};t\right)\right|^2 dt} \tag{6}$$

where

- $\Psi_{tot}^{(v)}\left(\mathbf{r}_m^{(v)};t\right)$ is the time-domain total field measured by the m-th probe under the v-th view, at time instant t;
- $\nu^{(v)}\left(\mathbf{r}_m^{(v)};t\right)$ is the noise component affecting the total field total field measured by the m-th probe under the v-th view, at time instant t;

1.4.1 Measuring the resulting SNR on frequency-domain scattered field

After the total measured field has been corrupted in time-domain by a given quantity of noise (following the above definition of SNR), the scattered field is obtained - in the frequency domain - as the difference between the transformed total and incident fields. The resulting SNR at a given frequency f on the external scattered field can be estimated as the average SNR measured over all the views $v = 1, ..., V$:

$$SNR\left\{E_{scatt}\left(f\right)\right\} = \frac{1}{V}\sum_{v=1}^{V} SNR\left\{E_{scatt}^{(v)}\left(f\right)\right\} \tag{7}$$

where $SNR\left\{E_{scatt}^{(v)}\left(f\right)\right\}$ represents the Signal-To-Noise Ratio measured on the scattered field in frequency domain for a given view v $(v = 1, ..., V)$ and it can be measured as:

$$SNR\left\{E_{scatt}^{(v)}\left(f\right)\right\} = 10log_{10}\left\{\frac{\sum_{m=1}^{M}\left|E_{scatt}^{(v),noiseless}\left(\mathbf{r}_m^{(v)};f\right)\right|^2}{\sum_{m=1}^{M}\left|n^{(v)}\left(\mathbf{r}_m^{(v)};f\right)\right|^2}\right\} \tag{8}$$

where the noise component $n^{(v)}\left(\mathbf{r}_m^{(v)};f\right)$ on a given measurement point m is computed as the difference between the noisy and the noiseless realizations of the scattered field measured on that point (for a given view v):

$$n^{(v)}\left(\mathbf{r}_m^{(v)};f\right) = E_{scatt}^{(v)}\left(\mathbf{r}_m^{(v)};f\right) - E_{scatt}^{(v),noiseless}\left(\mathbf{r}_m^{(v)};f\right). \tag{9}$$

ELEDIA Research Center

1.5 Reconstruction errors

The following integral error is defined

$$\Xi_{reg} = \frac{1}{N_{reg}} \sum_{n=1}^{N_{reg}} \frac{|\tau_n^{act} - \tau_n^{rec}|}{|\tau_n^{act} + 1|} \tag{10}$$

where reg indicates if the error computation covers

- the overall investigation domain ($reg \Rightarrow tot$),
- the actual scatterer support ($reg \Rightarrow int$),
- or the background region ($reg \Rightarrow ext$).

ELEDIA Research Center

1.6 $FH-IMSA-PSO$: Passing the solution from frequency to frequency

1. First frequency step ($f = f_1$): the reconstruction for the first $FH-IMSA-PSO$ step ($s = 1$) is initialized using:

   - Initial guess for $\tau(\mathbf{r}; f_1)$: **background**

   $$\tau(\mathbf{r}; f_1)|_{s=0} = 0$$

   - Initial guess for the internal total field $E_{tot}^{int}(\mathbf{r}; f_1)$: use the **internal incident field** computed by $GPRMAX$ for current frequency:

   $$E_{tot,int}^{(v)}(\mathbf{r}; f_1)\Big|_{s=0} = E_{inc,int}^{(v)}(\mathbf{r}; f_1)$$

2. Successive frequency steps ($f_1 > f \geq f_F$): the reconstruction for the first $FH-IMSA-PSO$ step ($s = 1$) is initialized using:

   - Initial guess for $\tau(\mathbf{r}; f_i)$: **map the final reconstruction** obtained at the best $FH-IMSA-PSO$ step ($s = s^{best}$) at the previous frequency ($f = f_{i-1}$) (after proper re-scaling of the solution to the full investigation domain D_{ind}) to the current frequency

   $$\tau(\mathbf{r}; f_i)|_{s=0} = \Re\{\tau(\mathbf{r}; f_{i-1})|_{s=s^{best}}\} + j\left[\frac{f_{i-1}}{f_i}\right]\Im\{\tau(\mathbf{r}; f_{i-1})|_{s=s^{best}}\}$$

   - Initial guess for the internal total field $E_{tot}^{int}(\mathbf{r}; f_1)$: use a $2D$ subsurface MoM (Ω) to compute the internal total field at $f = f_i$ using the initial guess of $\tau(\mathbf{r}; f_i)|_{s=0}$:

   $$E_{tot}^{int}(\mathbf{r}; f_1)\big|_{s=0} = \Omega\{\tau(\mathbf{r}; f_i)|_{s=0}\}.$$

1.6.1 Re-scaling $\tau(\mathbf{r}; f_{i-1})|_{s=s^{best}}$ to the original domain extension

When jumping from frequency f_{i-1} to frequency f_i , the final reconstruction obtained at the best step (s^{best}) of frequency f_{i-1} must be re-scaled to the whole original domain (D_{ind}). This is done by considering a **weighted average** of its pixels.

The n-th pixel ($n = 1, ..., N$) of $\tau(\mathbf{r}; f_{i-1})|_{s=s^{best}}$ is computed as:

$$\tau(x_n, y_n; f_{i-1})|_{s=s^{best}} = \sum_{j=1}^{J_n}\left(\frac{A_{j,n}}{A_n}\right)\hat{\tau}(x_j, y_j; f_{i-1})|_{s=s^{best}}$$

where:

FEEDIA Research Center

- $(x_n, y_n) \in D^{ind}$, $n = 1, ..., N$;
- $\hat{\tau}(x_j, y_j; f_{i-1})|_{s=s^{best}}$ is the j-th pixel of the final reconstruction obtained at step $s = s^{best}$ at frequency f_{i-1}, before re-scaling ($(x_j, y_j) \in D^{zoomed}_{f_{i-1}, s=s^{best}}$, $i = 1, ..., N$);
- J_n is the number of cells of $\hat{\tau}(x_j, y_j; f_{i-1})|_{s=s^{best}}$ overlapping (even partially) with the n-th cell of $\tau(\mathbf{r}; f_{i-1})|_{s=s^{best}}$;
- $A_n = \left(\frac{L_{D_{inv}}}{N}\right)^2$ is the area of the n-th pixel of $\tau(x_n, y_n; f_{i-1})|_{s=s^{best}}$ $(n = 1, ..., N)$;
- $A_{j,n}$ is the area of the overlapping region between the j-th pixel of $\hat{\tau}(x_j, y_j; f_{i-1})|_{s=s^{best}}$ and the n-th pixel of $\tau(\mathbf{r}; f_{i-1})|_{s=s^{best}}$.

ELEDIA Research Center

2 $FH-BARE-PSO$ vs. $FH-IMSA-PSO$: Preliminary Numerical Validation

2.1 Goal of this section

This section is aimed at verifying the correct implementation of the following solvers

1. $FH-BARE-PSO$
2. $FH-IMSA-PSO$

when dealing with a single homogeneous scatterer and noiseless data.

ELEDIA Research Center

2.2 Case $N^{IMSA} = 196$, $N^{BARE} = 400$, $V = 20$, $M = 19$

2.2.1 Parameters

Background

Inhomogeneous and nonmagnetic background composed by two half spaces

- Upper half space ($y > 0$ - air): $\varepsilon_{ra} = 1.0$, $\sigma_a = 0.0$;
- Lower half space ($y < 0$ - soil): $\varepsilon_{rb} = 4.0$, $\sigma_b = 10^{-3}$[S/m];

Investigation domain (D_{inv})

- Side: $L_{D_{inv}} = 0.8$ [m];
- Barycenter: $\left(x_{bar}^{D_{inv}}, y_{bar}^{D_{inv}}\right) = (0.00, -0.4)$ [m];

Time-Domain forward solver ($FDTD$ - $GPRMax2D$)

- Side of the simulated domain: $L^{FDTD} = 6$ [m];
- Number of cells: $N^{FDTD} = 750 \times 750 = 5.625 \times 10^5$;
- Side of the $FDTD$ cells $l^{FDTD} = 0.008$ [m];
- Simulation time window: $T^{FDTD} = 20 \times 10^{-9}$ [sec];
- Time step: $\Delta t^{FDTD} = 1.89 \times 10^{-11}$ [sec];
- Number of time samples: $N_t^{FDTD} = 1060$;
- Boundary conditions: perfectly matched layer (PML);
- Source type: Gaussian mono-cycle (first Gaussian pulse derivative, called "Ricker" in $GPRMax2D$)
  - Central frequency: $f_0 = 300$ [MHz];
  - Source amplitude: $A = 1.0$ [A];

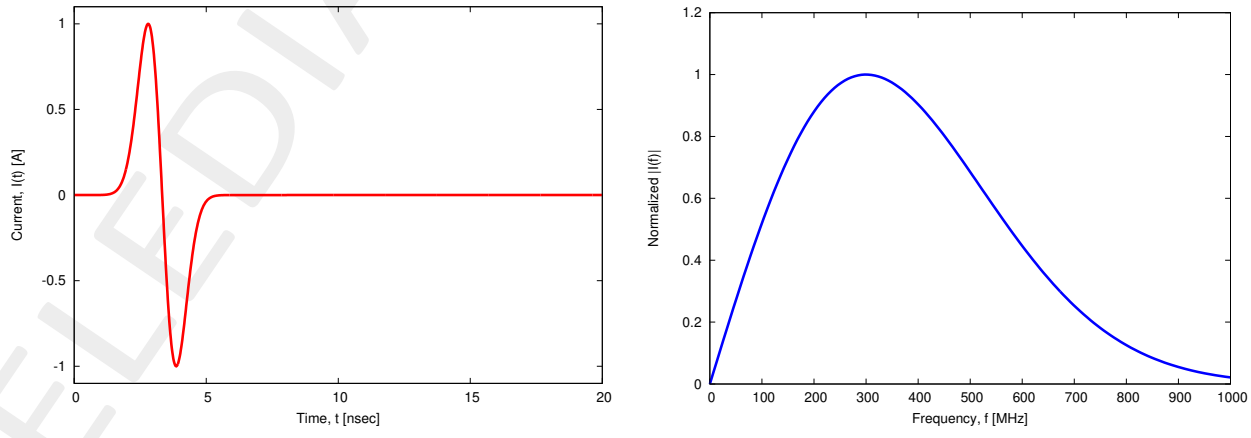

(a) (b)

Figure 1: $GPRMax2D$ excitation signal. (a) Time pulse, (b) normalized frequency spectrum.

ELEDIA Research Center

Frequency parameters

- Frequency range: $f \in [f_{min}, f_{max}] = [200.0, 600.0]$ [MHz];
- Frequency step: $\Delta f = 100$ [MHz] ($F = 5$ frequency steps in $[f_{min}, f_{max}]$);

f [MHz]	λ_a [m]	λ_b [m]	f^* [MHz]
200.0	1.50	0.75	200.5
300.0	1.00	0.50	297.6
400.0	0.75	0.37	401.1
500.0	0.60	0.30	498.1
600.0	0.50	0.25	601.6

Table 1: Considered frequencies and corresponding wavelength in the upper medium (λ_a, free space) and in the lower medium (λ_b, soil). f^* is the nearest frequency sample available from transformed time-domain data, and represents the real frequency considered by the inversion algorithm.

Scatterer

- Type: square-shaped;
- Barycenter: $(x_{obj}, y_{obj}) = (-0.08, -0.24)$ [m];
- Side: $L_{obj,x} = L_{obj,y} = 0.16$ [m];
- Electromagnetic properties: $\varepsilon_{r,obj} = 5.0$, $\sigma_{obj} = 10^{-3}$ [S/m] ($\sigma_{obj} = \sigma_b$);
- Contrast function: $\tau = 1.0 + j0.0$

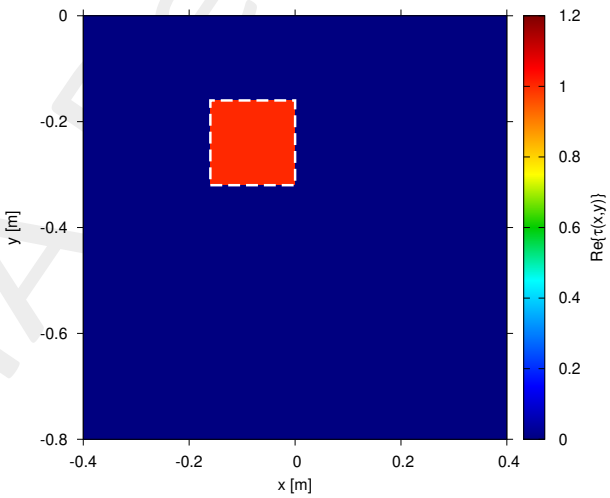

Figure 2: Actual object: offset square cylinder $\tau = 1.0$.

ELEDIA Research Center

Measurement setup

- Considered frequency: $f_{central} = 400$ [MHz], $\lambda_b = 0.37$ [m];
- $\#DoFs = 2ka = \frac{2\pi}{\lambda_b} L\sqrt{2} = \frac{2\pi}{0.37} 0.8\sqrt{2} \simeq 19.2$;
- Number of views (sources): $V = 20$;
  - $\min\{x_v\} = -0.564$ [m], $\max\{x_v\} = 0.5$ [m];
  - height: $y_v = 0.1$ [m], $\forall v = 1, \ldots, V$;
- Number of measurement points: $M = 19$;
  - $\min\{x_m\} = -0.564$ [m], $\max\{x_m\} = 0.5$ [m];
  - height: $y_m = 0.1$ [m], $\forall m = 1, \ldots, M$;

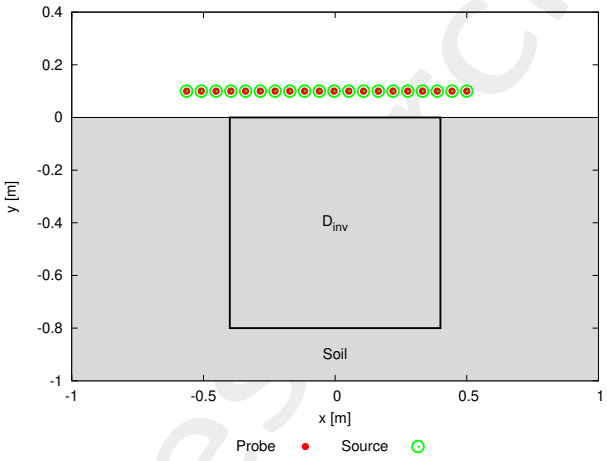

Figure 3: Location of the measurement points ($M = 19$) and of the sources ($V = 20$). Only one source is active for each view.

Inverse solver parameters

- **Shared parameters**
  - Weight of the state term of the functional: 1.0;
  - Weight of the data term of the functional: 1.0;
  - Weight of the penalty term of the functional: 0.0;
  - Convergence threshold: 10^{-10};
  - Variable ranges:
    - $\varepsilon_r \in [4.0, 6.0]$, $\sigma \in \left[0.0, 2 \times 10^{-3}\right]$ [S/m];
    - $\Re\left\{E_{tot}^{int}\right\} \in [-25, 25]$, $\Im\left\{E_{tot}^{int}\right\} \in [-25, 25]$;
  - $C_1 = C_2 = 2.0$;

ELEDIA Research Center

- Inertial weight: $w = 0.4$;
- Velocity clamping: disabled;

- $FH - BARE - PSO$ **parameters**
  - Frequency-hopping strategy: FH-FULL;
  - Number of cells: $N = 20 \times 20 = 400$;
  - Side of the cells: $l = 0.04$ [m] $\rightarrow \sim \lambda_b/10$ discretization @ $f_{central} = 400$ [MHz];
  - Maximum number of iterations: $I = 2000$;
  - Number of unknowns: $U = 2N\,(1 + V) = 16800$;
  - Swarm dimension: $P = \frac{5}{100} \times U = 840$;

- $FH - IMSA - PSO$ **parameters**
  - Frequency-hopping strategy: FH-FULL Area-Based;
  - Degrees of freedom:
    - Considered frequency: $f_{central} = 400$ [MHz], $\lambda_b = 0.37$ [m];
    - $\frac{(2ka)^2}{2} = \frac{\left(2 \times \frac{2\pi}{\lambda_b} \times \frac{L\sqrt{2}}{2}\right)^2}{2} = 4\pi^2 \left(\frac{L}{\lambda_b}\right)^2 = 4\pi^2 \left(\frac{0.8}{0.37}\right)^2 \simeq 184.4$;
  - Number of cells: $N = 196 = 14 \times 14$;
  - Side of the cells ($s = 1$): $l = 0.057$ [m];
  - Maximum number of $IMSA$ steps: $S = 4$;
  - Side ratio threshold: $\eta_{th} = 0.2$;
  - Maximum number of iterations: $I = 2000$;
  - Number of unknowns: $U = 2N\,(1 + V) = 8232$;
  - Swarm dimension: $P = \frac{5}{100} \times U = 412$;

Signal to noise ratio (SNR)

- Noiseless data.

ELEDIA Research Center

2.2.2 $FH-BARE-PSO$ vs. $FH-IMSA-PSO$: Reconstructions

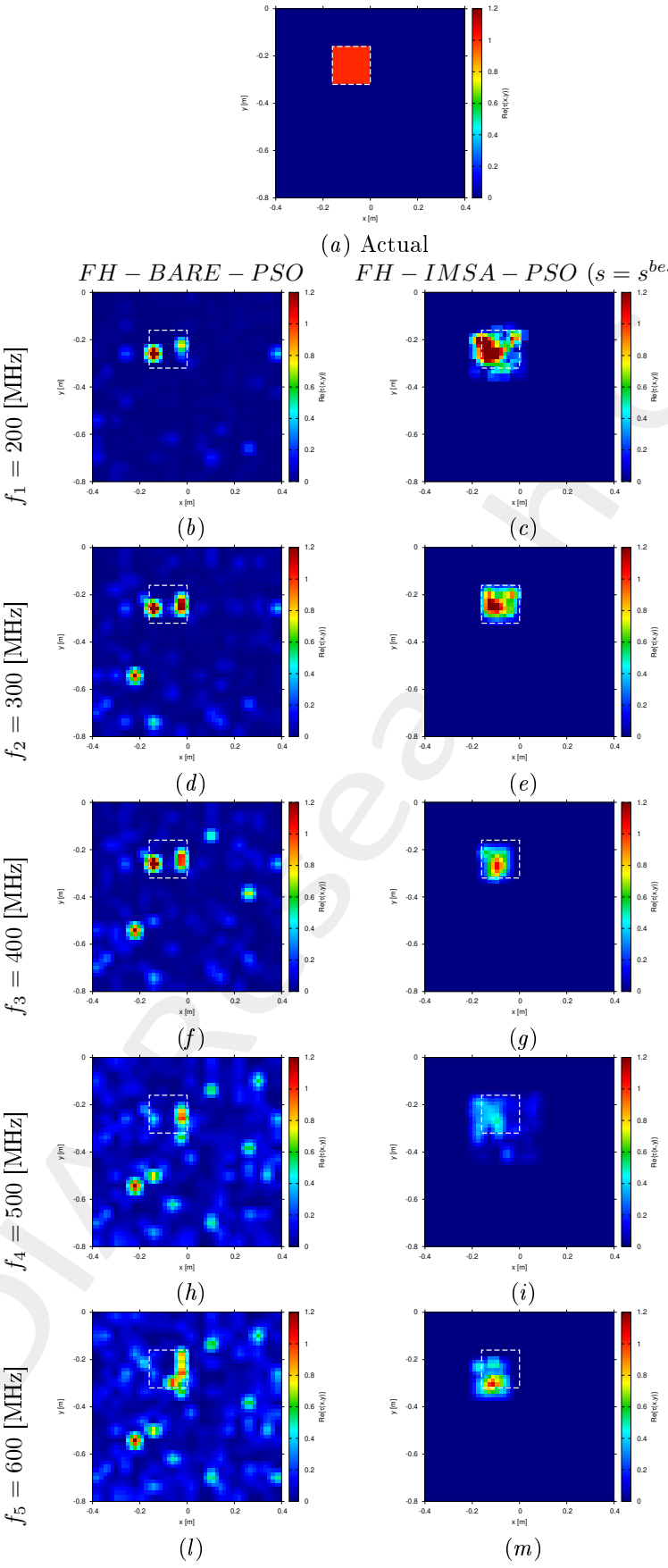

Figure 4: $FH-BARE-PSO$ vs. $FH-IMSA-PSO$: Retrieved dielectric profiles at each intermediate frequency step.

FLEDIR Research Center

2.2.3 $FH-IMSA-PSO$: All intermediate reconstructions

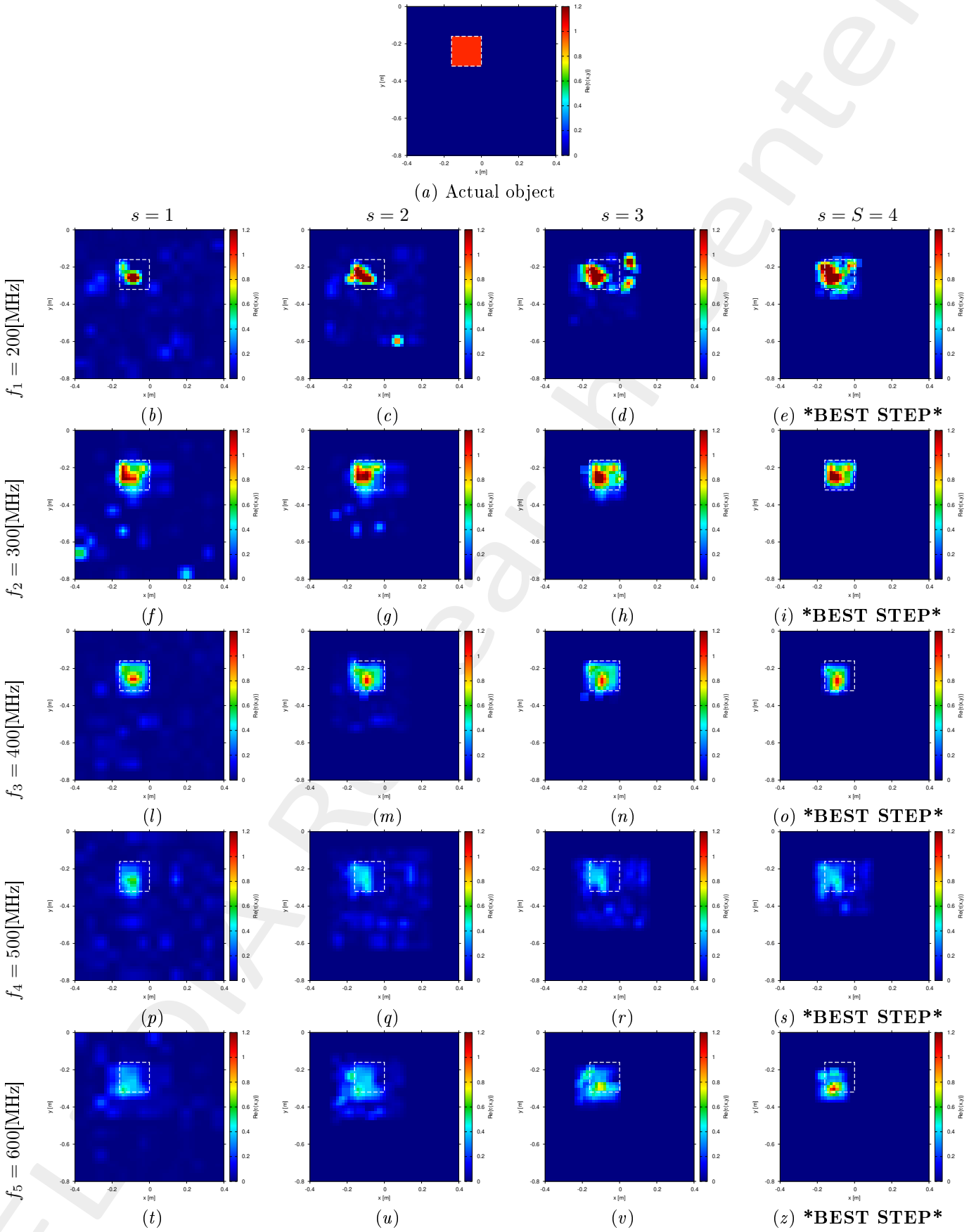

Figure 5: $FH-IMSA-PSO$: Actual object and reconstructions for all $IMSA$ steps and all frequency steps in $f \in [200, 600]$ [MHz].

Fl. DIA Radar Preenter

2.2.4 Fitness evolution

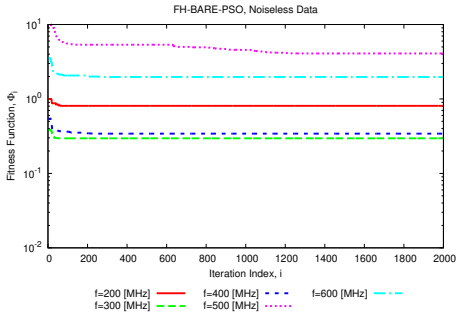

Figure 6: $FH-BARE-PSO$: Fitness evolution at each frequency stage.

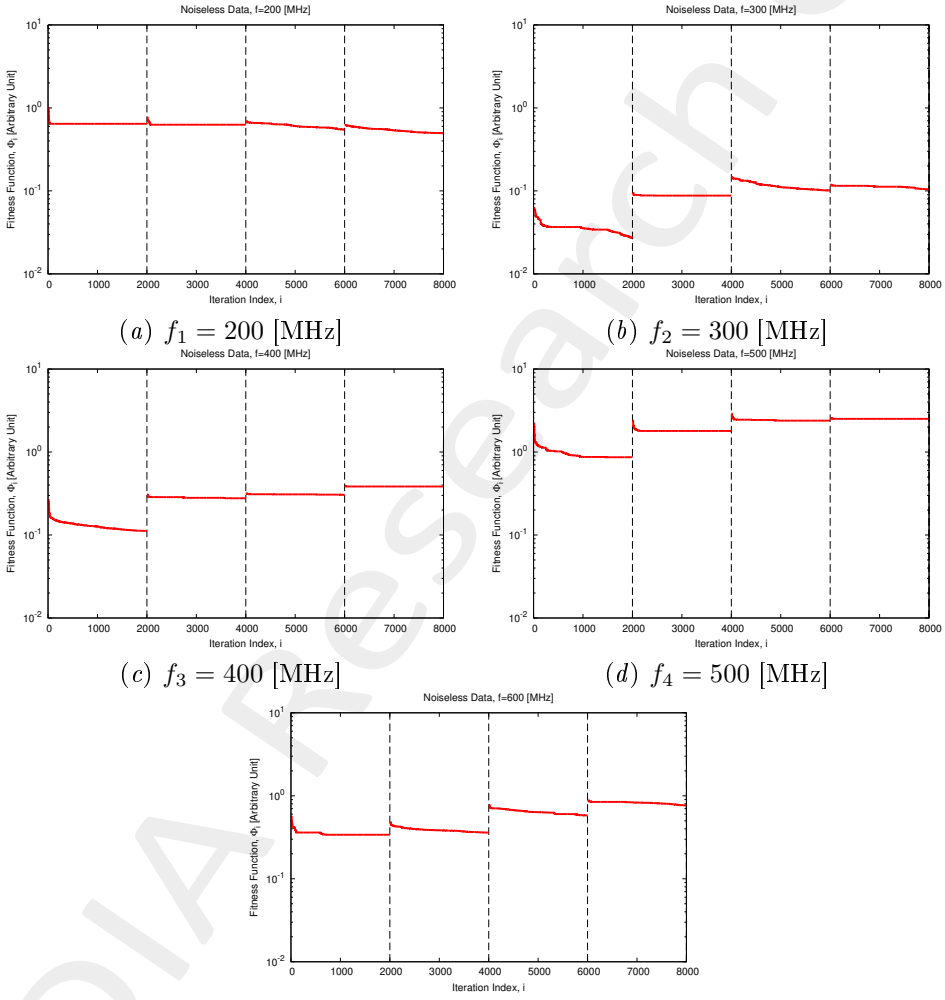

(a) $f_1 = 200$ [MHz] (b) $f_2 = 300$ [MHz]

(c) $f_3 = 400$ [MHz] (d) $f_4 = 500$ [MHz]

(e) $f_5 = 600$ [MHz]

Figure 7: $FH-IMSA-PSO$: Fitness evolution at each $IMSA$ step at each frequency stage.

ELEDIA Research Center

2.2.5 Reconstruction errors

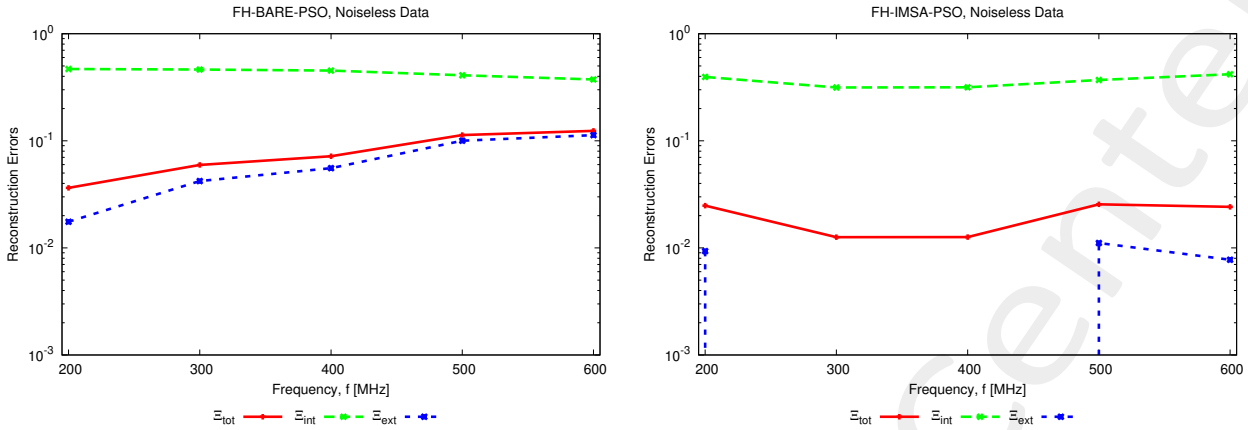

(a) $FH-BARE-PSO$ (b) $FH-IMSA-PSO$

Figure 8: $FH-BARE-PSO$ vs. $FH-IMSA-PSO$: Evolution of the reconstruction errors vs. frequency step.

	$FH-BARE-PSO$			$FH-IMSA-PSO$			
	Ξ_{tot}	Ξ_{int}	Ξ_{ext}	s^{best}	Ξ_{tot}	Ξ_{int}	Ξ_{ext}
$f_1 = 200$ [MHz]	3.63×10^{-2}	4.68×10^{-1}	1.75×10^{-2}	4	2.48×10^{-2}	3.95×10^{-1}	9.33×10^{-3}
$f_2 = 300$ [MHz]	5.95×10^{-2}	4.63×10^{-1}	4.21×10^{-2}	4	1.26×10^{-2}	3.15×10^{-1}	0.00
$f_3 = 400$ [MHz]	7.18×10^{-2}	4.53×10^{-1}	5.54×10^{-2}	4	1.26×10^{-2}	3.16×10^{-1}	0.00
$f_4 = 500$ [MHz]	1.13×10^{-1}	4.09×10^{-1}	1.00×10^{-1}	4	2.55×10^{-2}	3.70×10^{-1}	1.11×10^{-2}
$f_5 = 600$ [MHz]	1.24×10^{-1}	3.74×10^{-1}	1.13×10^{-1}	4	2.42×10^{-2}	4.18×10^{-1}	7.75×10^{-3}

Table 2: Final reconstruction errors computed for the different approaches.

ELEDIA Research Center

More information on the topics of this document can be found in the following list of references.

References

[1] P. Rocca, M. Benedetti, M. Donelli, D. Franceschini, and A. Massa, ”Evolutionary optimization as applied to inverse problems,” *Inverse Probl.*, vol. 25, pp. 1-41, Dec . 2009 (DOI: 10.1088/0266-5611/25/12/123003).

[2] P. Rocca, G. Oliveri, and A. Massa, "Differential Evolution as applied to electromagnetics," *IEEE Antennas Propag. Mag.*, vol. 53, no. 1, pp. 38-49, Feb. 2011 (DOI: 10.1109/MAP.2011.5773566).

[3] Salucci, G. Oliveri, and A. Massa, "GPR prospecting through an inverse scattering frequency-hopping multi-focusing approach," *IEEE Trans. Geosci. Remote Sens.*, vol. 53, no. 12, pp. 6573-6592, Dec. 2015 (DOI: 10.1109/TGRS.2015.2444391).

[4] M. Salucci, L. Poli, and A. Massa, "Advanced multi-frequency GPR data processing for non-linear deterministic imaging," *Signal Processing - Special Issue on "Advanced Ground-Penetrating Radar Signal-Processing Techniques*," vol. 132, pp. 306-318, Mar. 2017 (DOI: 10.1016/j.sigpro.2016.06.019).

[5] M. Salucci, L. Poli, N. Anselmi, and A. Massa, "Multifrequency particle swarm optimization for enhanced multiresolution GPR microwave imaging," *IEEE Trans. Geosci. Remote Sens.*, vol. 55, no. 3, pp. 1305-1317, Mar. 2017 (DOI: 10.1109/TGRS.2016.2622061).

[6] A. Massa, P. Rocca, and G. Oliveri, "Compressive sensing in electromagnetics - A review," *IEEE Antennas Propag. Mag.*, pp. 224-238, vol. 57, no. 1, Feb. 2015 (DOI: 10.1109/MAP.2015.2397092).

[7] A. Massa and F. Texeira, Guest-Editorial: Special Cluster on Compressive Sensing as Applied to Electromagnetics, *IEEE Antennas Wireless Propag. Lett.*, vol. 14, pp. 1022-1026, 2015 (DOI: 10.1109/LAWP.2015.2425011).

[8] N. Anselmi, G. Oliveri, M. Salucci, and A. Massa, "Wavelet-based compressive imaging of sparse targets," *IEEE Trans. Antennas Propag.*, vol. 63, no. 11, pp. 4889-4900, Nov. 2015 (DOI: 10.1109/TAP.2015.2444423).

[9] G. Oliveri, N. Anselmi, and A. Massa, "Compressive sensing imaging of non-sparse 2D scatterers by a total-variation approach within the Born approximation," *IEEE Trans. Antennas Propag.*, vol. 62, no. 10, pp. 5157-5170, Oct. 2014 (DOI: 10.1109/TAP.2014.2344673).

[10] T. Moriyama, G. Oliveri, M. Salucci, and T. Takenaka, "A multi-scaling forward-backward time-stepping method for microwave imaging," *IEICE Electron. Expr.*, vol. 11, no. 16, pp. 1-12, Aug. 2014 (DOI: 10.1587/elex.11.20140578).

[11] T. Moriyama, M. Salucci, M. Tanaka, and T. Takenaka, "Image reconstruction from total electric field data with no information on the incident field," *J. Electromagnet. Wave.*, vol. 30, no. 9, pp. 1162-1170, 2016 (DOI: 10.1080/09205071.2016.1182876).

[12] F. Viani, L. Poli, G. Oliveri, F. Robol, and A. Massa, "Sparse scatterers imaging through approximated multi-task compressive sensing strategies," *Microw. Opt. Technol. Lett.*, vol. 55, no. 7, pp. 1553-1557, Jul. 2013 (DOI: 10.1002/mop.27612).

[13] M. Salucci, N. Anselmi, G. Oliveri, P. Calmon, R. Miorelli, C. Reboud, and A. Massa, "Real-time NDT-NDE through an innovative adaptive partial least squares SVR inversion approach," *IEEE Trans. Geosci. Remote Sens.*, vol. 54, no. 11, pp. 6818-6832, Nov. 2016 (DOI: 10.1109/TGRS.2016.2591439).

[14] L. Poli, G. Oliveri, and A. Massa, "Imaging sparse metallic cylinders through a local shape function bayesian compressing sensing approach," *J. Opt. Soc. Am. A*, vol. 30, no. 6, pp. 1261-1272, Jun. 2013 (DOI: 10.1364/JOSAA.30.001261).

[15] M. Donelli, D. Franceschini, P. Rocca, and A. Massa, "Three-dimensional microwave imaging problems solved through an efficient multiscaling particle swarm optimization," *IEEE Trans. Geosci. Remote Sensing*, vol. 47, no. 5, pp. 1467-1481, May 2009 (DOI: 10.1109/TGRS.2008.2005529).